

# Poole-Frenkel electron emission from the traps in AlGaIn/GaN transistors

Oleg Mitrofanov and Michael Manfra

*Bell Laboratories, Lucent Technologies, 600 Mountain Avenue, Murray Hill, New Jersey 07974*

(Received 26 January 2004; accepted 3 March 2004)

Defect-related localized electronic states in AlGaIn/GaN transistors give rise to commonly observed charge trapping phenomena. Electron dynamics through the trapping centers is strongly affected by electric fields, which can exceed values of  $10^6$  V/cm during device operation. The field-assisted emission characteristics provide a unique way to determine the physical properties of the trapping centers. We present a detailed study of the effects of electric field and temperature on the rate of electron emission from the barrier traps in AlGaIn/GaN high-electron-mobility transistors. We demonstrate that for temperatures above 250 K, the Poole-Frenkel (PF) emission is the dominant mechanism for electrons to escape from the trapping centers. The emission rate increases exponentially with the square root of the applied field consistent with the decrease of the apparent activation energy predicted by the PF model. We find that the observed trapping center is described by the attractive long-range Coulomb potential with the zero-field binding energy of  $\sim 0.5$  eV.

© 2004 American Institute of Physics. [DOI: 10.1063/1.1719264]

## I. INTRODUCTION

Defects and impurities introduce localized electronic states in semiconductors. Energy levels of some states lie within the semiconductor band gap. GaN is known to contain a large density of defects and dislocations because of the lack of a native substrate. In addition, it is believed that ionized donor states are located on the surface of AlGaIn.<sup>1,2</sup> The localized states can act as charge trapping centers in the structure of semiconductor devices, becoming a limiting factor with regard to the device performance. The trapping effects are commonly observed in the characteristics of GaN-based high-electron-mobility transistors (HEMTs).<sup>3</sup> Particularly, in AlGaIn/GaN HEMTs, the modulation of the gate potential results in electron trapping in the vicinity of the gate electrode.<sup>4</sup> The field of the trapped electrons partially depletes the two-dimensional electron gas (2DEG) in the channel and limits the source-drain current. The origin of the active traps and their spatial location are currently disputed. Considerable disagreement in the field arises because of difficulties of accurate quantitative characterization of the defects in the actual devices and wide variation of the material quality between different groups. There is no doubt that the understanding of the role of the defects and the mechanisms of the defect formation is required to improve GaN technology. The critical step toward understanding the trapping phenomena is the identification of the trapping centers, characterization of their activation energies, and determining the spatial location in the actual devices.

Impurity or defect states are identified by their signatures: charge state, ionization energy, and the capture cross section. These characteristics can be deduced by analyzing the emission rate of the trapped charge from the defects.<sup>5</sup> For instance, the ionization energy  $E_T$  of a localized level within the band gap is related to the rate of thermally activated ionization,  $e$ , by an Arrhenius-type relationship. The ionization energy, therefore, can be found by analyzing the func-

tional dependence of the rate on the temperature. In the presence of an electric field, the relationship between  $e$  and  $E_T$  becomes more complicated. The rate of charge emission from the traps located in the field region can substantially increase because of the potential barrier lowering,<sup>6</sup> direct tunneling, and phonon-assisted tunneling.<sup>7</sup> In AlGaIn/GaN HEMTs, the electric field strength in the barrier can exceed values of  $10^6$  V/cm. Electron emission from the traps located in the barrier is therefore strongly influenced by the field.<sup>8</sup> Consequently, the electric field enhancement has to be taken into account to determine an accurate value of the zero-field ionization energy of the defects.

In this paper we present a detailed study of the thermal and electric field dependence of the emission process from an electron trap in GaN/AlGaIn/GaN high-electron-mobility transistors. The functional dependence of the emission rate on the applied field and the temperature allows unambiguous identification of the Poole-Frenkel (PF) emission mechanism at room temperature. In particular, we demonstrate that the emission rate increases exponentially with the square root of the applied field and that the apparent activation energy consistently decreases with the field. Understanding the nature of the process allows an accurate estimation of the zero-field ionization energy, which differs significantly from the apparent activation energy in the presence of the very high electric field ( $\sim 10^6$  V/cm). The functional dependence of the emission rate on the applied field implies that the ionized trapping centers are positively charged and they are characterized by Coulomb long-range potential. Furthermore, we estimate the electric field strength acting on the traps and identify their spatial location.

## II. FIELD ENHANCED EMISSION

We first consider mechanisms that enhance the rate of charge emission from trapping centers. In equilibrium, a system of trapping centers maintains a constant density of local-

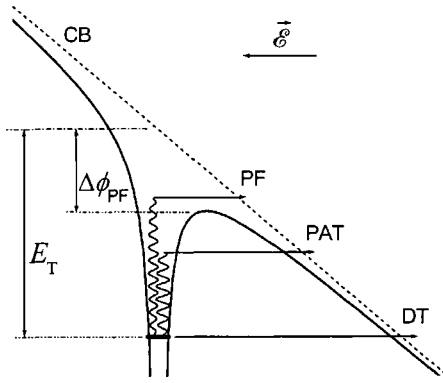


FIG. 1. Energy diagram of the trapping center in the presence of the electric field. Arrows indicate the possible mechanisms of electron emission: thermal ionization over the lowered barrier (PF effect), direct tunneling (DT) into the conduction band (CB), and phonon assisted tunneling (PAT).

ized electrons, determined by balancing of the emission and the capture processes. Using the principle of detailed equilibrium and assuming that the emission process is thermally activated, one finds that the emission rate from the deep levels in the semiconductor band gap,  $e$ , is related to the ionization energy  $E_i$  by the Arrhenius equation<sup>9</sup>

$$e = AT^2 \exp\left(-\frac{E_i}{kT}\right), \quad (1)$$

In the presence of the electric field, efficiencies of the capture and emission processes may change, leading to a new equilibrium number of the trapped electrons. The effect of the electric field is illustrated in Fig. 1 for a trap described by the Coulomb long-range potential. In the direction of the applied field, the potential barrier is lowered. An electron now requires less energy to escape from the trap. This mechanism of the field-assisted emission is known as the Poole-Frenkel effect. The barrier decreases by an amount  $\Delta\phi_{PF}$  proportional to the square root of the applied electric field  $F$ ,

$$\Delta\phi_{PF} = \left(\frac{q^3}{\pi\epsilon}\right)^{1/2} \sqrt{F} = \beta\sqrt{F}, \quad (2)$$

where  $q$  is a unit of electron charge, and  $\epsilon$  is the dielectric constant of the material.<sup>5</sup> The ionization energy  $E_i$  appearing in the emission rate equation becomes field dependent,

$$E_i(F) = E_i(0) - \beta\sqrt{F}, \quad (3)$$

where  $E_i(0) = E_T$  is the binding energy of the electron on the trap in the zero field. Evaluation of this expression suggests that the activation energy of the traps located in the region of high electric field ( $10^6$  V/cm) can be up to 0.2–0.25 eV smaller than the zero-field binding energy. As a result, the rate of electron emission from the trap is strongly enhanced by the field:  $e(F) = e(0)\exp(\Delta\phi_{PF}/kT)$ , increasing exponentially with the square root of the field.

In addition to the enhancement of the thermal ionization, the applied field increases the probability for the trapped electron to escape into the conduction band via tunneling processes (Fig. 1). If the bands are sufficiently tilted, a trapped electron can either directly tunnel through the barrier

or first acquire energy from the lattice and then tunnel out through a thinner barrier (phonon-assisted tunneling).<sup>7</sup> In the presence of alternative emission processes, the relationship between the emission rate and the ionization energy described by Eq. (1) does not capture all of the physics.

The relative efficiencies of the aforementioned emission mechanisms depend on the temperature. The direct tunneling is temperature independent and, therefore, it is the dominant mechanism at low temperatures. As the temperature increases, the electron can escape from the trap through absorption of a phonon. The pure thermal ionization becomes more efficient at the elevated temperatures and it eventually dominates the electron emission from the traps. Equation (1) therefore describes the emission rate in the high-temperature limit.

### III. EXPERIMENT

In our experiments, the trapping dynamics is studied in GaN/AlGaIn/GaN HEMTs grown by plasma-assisted molecular beam epitaxy (MBE) on semi-insulating SiC substrates. The heterostructure consists of  $\sim 2$   $\mu\text{m}$  thick GaN buffer layer, a 30 nm  $\text{Al}_{0.34}\text{Ga}_{0.66}\text{N}$  barrier, and a 5 nm GaN capping layer. Strong piezoelectric and spontaneous polarization effects result in a formation of the 2DEG at the AlGaIn/GaN interface. The density of the 2DEG is  $\sim 1.2 \times 10^{13} \text{ cm}^{-2}$  and the room temperature mobility is  $\sim 1400 \text{ cm}^2/\text{Vs}$ . The transistors are fabricated from the epilayers using optical contact lithography. A 1  $\mu\text{m}$  long Schottky gate is deposited in the middle of the 5  $\mu\text{m}$  long source-drain opening. Devices fabricated from three different wafers (A, B, and C) grown at similar conditions will be discussed. In sample C, the top 15 nm of the barrier layer and the GaN capping layer are doped with Si at a level  $10^{18} \text{ cm}^{-3}$ . The devices fabricated from all the wafers have the same design and are processed similarly. The details of MBE growth as well as large signal device performance have been discussed elsewhere.<sup>10–14</sup> The trapping effects observed in the devices fabricated from different wafers are similar. However, the amplitude of the effects in the undoped devices is typically larger as compared to the devices with the doped barrier.<sup>15</sup>

The dynamics of the electrons moving in and out of the traps is probed by measuring the induced charge in the transistor channel.<sup>8</sup> First, electrons are injected into the traps by applying a short negative filling pulse to the gate. The barrier height of the Schottky gate contact is sufficiently large ( $\sim 1.0$ – $1.5$  eV), such that the probability of electron transfer by thermal activation is small. However, during the filling pulse, there is a large field across the AlGaIn barrier, which allows electrons to tunnel from the gate into the semiconductor. The number of the trapped electrons increases rapidly with the duration of the filling pulse and then saturates after  $\sim 10$   $\mu\text{s}$ .<sup>8</sup> In these experiments, however, filling pulses with duration of 1  $\mu\text{s}$  and shorter are used to obtain trapped charge densities lower than the saturation level and to avoid emission enhancement due to Coulomb repulsion. As the gate potential returns to the initial value, the flow of electrons from the gate reduces and the concentration of the

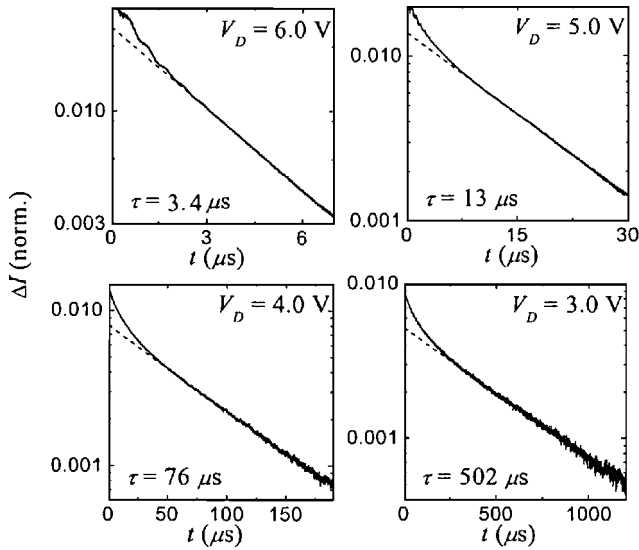


FIG. 2. Normalized current difference  $\Delta I$  measured after the filling pulse ( $V_G = -3$  V and  $\tau_p = 350$  ns) for different drain voltages in sample A. The dashed line shows the exponential fit to the tail of the transient.

trapped electrons slowly returns to the equilibrium through emission processes.

The emission dynamics is directly reflected in the channel current transients. The field of the trapped electrons induces partial depletion of the 2DEG. The electron density variation is proportional to the amount of the trapped charge.<sup>8</sup> If a potential difference is applied between the source and the drain, a channel current transient that follows the filling gate pulse reflects the process of electron emission from the traps. The rate of current approach to the steady state level corresponds to the rate of electron emission from the traps.

In the experiment, the device is constantly biased in the common source configuration. Initially, the transistor is open and a steady state current  $I_D^{SS}$  is flowing in the channel. A filling pulse is applied to the gate every 50 ms. The drain current transient following the filling pulse is measured by a low insertion impedance 100 MHz bandwidth current probe. The electric field in the barrier of the HEMT consists of two components: the internal spontaneous polarization and the piezoelectric field of the heterostructure and the external electric field due to the potential difference between the gate contact and the transistor channel. At the potential difference of few volts, the external electric field magnitude exceeds values of  $10^6$  V/cm and becomes the major contribution to the total electric field in the barrier. For traps located in the barrier, dependence of the emission rate on the electric field is obtained by varying the drain potential. In the linear current regime ( $V_D$  is smaller than the knee voltage), the field in the barrier is directly proportional to the potential difference between the gate and the drain.

Typical normalized current transients  $\Delta I(t) = I_D^{SS} - I_D(t)$  measured on wafer A at different drain bias conditions at room temperature are shown in Fig. 2. To fill the traps, a 350 ns long filling pulse  $V_G(t) = -3$  V is applied to the gate. The emission of the trapped charge that immediately follows the filling pulse is measured at  $V_G = 0$  V. All

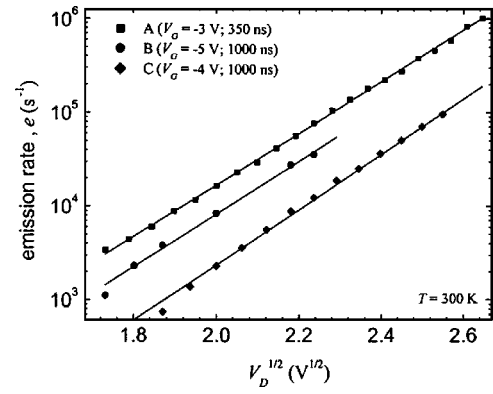


FIG. 3. Emission rate as a function of the square root of the applied voltage ( $V_D$ ). The depth and the duration of the filling pulses for samples A,  $V_G = -3$  V and  $\tau_p = 350$  ns; B,  $V_G = -5$  V and  $\tau_p = 1000$  ns; and C,  $V_G = -4$  V and  $\tau_p = 1000$  ns.

the transients obtained at different bias conditions show exponential approach to the steady state current level. The beginning of the transients contains a short nonexponential region, which we attribute to the emission enhancement due to the Coulomb repulsion. To obtain the emission rate, the long tail of the transient is fitted with the exponential decay function shown by the dashed line.

The characteristic emission time  $\tau = (e)^{-1}$  quickly decreases with the field strength  $F$ , suggesting that the emission from the trap is strongly assisted by the applied electric field. The functional dependence of the emission rate on the field is determined by fitting the data  $e(F)$  for sample A with a power law function ( $\ln e = a + bV^p$ ). The result of the fitting ( $p = 0.53$ ) suggests that the emission rate increases exponentially with the square root of the applied field. Figure 3 shows the emission rate as a function of the square root of the field measured on wafers A, B, and C. The solid lines in the plot show fits to the data:  $e = e(0)\exp(\alpha\sqrt{V_D})$ . The physical meaning of  $e(0)$  is the zero-field emission rate, and  $\alpha$  is a constant that relates the applied voltage and the lowering of the trap potential. The zero-field emission rate varies from  $0.04 \pm 0.03$  s<sup>-1</sup> for wafer A to  $0.003 \pm 0.001$  s<sup>-1</sup> for wafer C. On wafer variation of the emission rate (for different devices) is insignificant. The values of constant  $\alpha$  for different devices and wafers reside very closely to each other within the error bar  $\alpha = 6.6 \pm 0.5$  V<sup>-1/2</sup> ( $T = 300$  K).

The emission rate increases at elevated temperatures, suggesting the thermal nature of the emission process. The activation energy is found from the slope of the logarithmic plot of  $eT^2$  versus the inverse temperature. Figure 4 shows the emission rate for a sample on wafer C measured at the bias conditions ranging from  $V_D = 4.25$  V to  $V_D = 5.75$  V. The duration and the depth of the filling pulse are 1000 ns and  $-4$  V, respectively. In the temperature range of 250 K to 360 K the emission rate follows the Arrhenius behavior of Eq. (1). The extracted activation energy is shown in the inset; it decreases with the applied field from  $0.14 \pm 0.005$  eV at  $V_D = 4.25$  V to  $0.089 \pm 0.005$  eV at  $V_D = 5.75$  V. The preexponential factor  $A = 7 \pm 1$  s<sup>-1</sup> K<sup>-2</sup> remains constant at lower fields and it increases slightly to a level of  $10 \pm 2$  s<sup>-1</sup> K<sup>-2</sup> at  $V_D = 5.75$  V. As the temperature decreases below 200 K, the

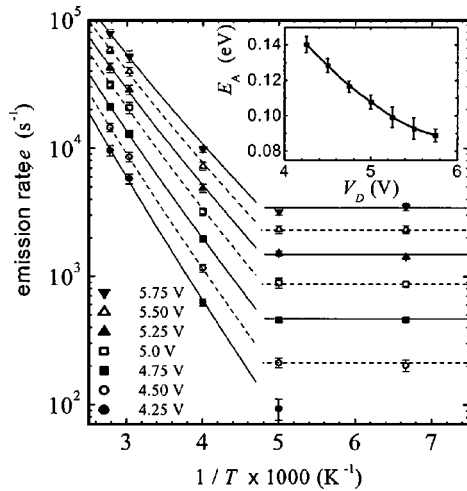


FIG. 4. The emission rate as a function of the inverse temperature measured at different drain voltages for sample C. The inset shows the activation energy extracted from the data in the high-temperature regime.

emission rate becomes temperature independent. This behavior can be attributed either to the presence of the competing emission mechanisms or to the device self-heating. For wafers A and B, we also observed the decrease of the activation energy with the applied field. Table I summarizes the experimental results for all samples.

#### IV. RESULTS AND DISCUSSIONS

##### A. Zero-field ionization energy

We showed that the electron emission agrees with Poole-Frenkel model of the trap barrier lowering in the field. Particularly, the rate of the emission process increases exponentially with the square root of the electric field. In addition, the temperature dependence confirms that the emission from the trap is thermal and the activation energy of the process decreases with the applied field. To identify the trap, we need to find a universal characteristic of the trap, such as the zero-field ionization energy. Knowing the mechanism of the emission enhancement, the zero-field ionization energy can be extrapolated from the activation energy data.

The thermally activated emission rate is described by the Arrhenius expression with the field dependent activation energy,

$$e(T, F) = AT^2 \exp\left[-\frac{E_T - \Delta\phi_{PF}(F)}{kT}\right], \quad (4)$$

where  $E_T$  is the zero-field ionization energy. The preexponential factor  $A$  was estimated by fitting the temperature corrected emission rate  $eT^{-2}$  with the exponential function of

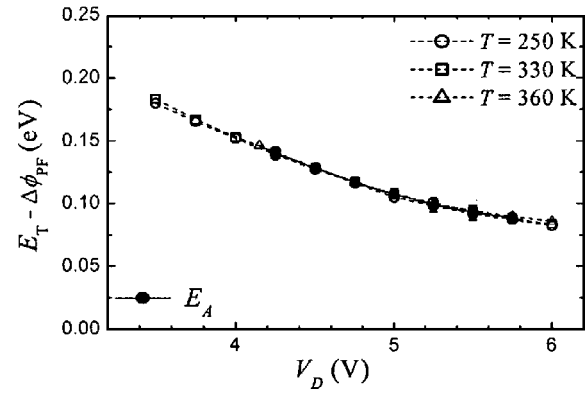


FIG. 5. The activation energy as a function of the applied voltage for sample C.

the inverse temperature (Fig. 4). For wafer C,  $A$  remains constant at different bias conditions. Therefore, we can express the activation energy in terms of the experimentally measured emission rate:  $E_i(F) = kT \ln[e(T, F)A^{-1}T^{-2}]$ . The results are plotted in Fig. 5 as open symbols. Excellent overlap between the curves obtained from the emission rate data at different temperatures confirms that the thermal emission is the dominant mechanism. In addition, the activation energy, experimentally extracted from the temperature variation of the emission rate (shown in solid circles), overlaps well with the data. The emission rate therefore is consistently described by Eq. (4), where the field dependence only enters the activation energy term.

The zero-field activation energy  $E_T$  is estimated by extrapolation of the data in Fig. 5 to  $V_D = 0$ , assuming that the activation energy continues following the square root dependence on the applied field and that the preexponential factor  $A$  remains constant at low fields. As mentioned earlier, the experimentally measured value of  $A$  is constant for wafers B and C. The extrapolated zero-field activation energy  $E_T$  is  $0.54 \pm 0.05$  eV for wafer C and  $0.41 \pm 0.05$  eV for wafer B. In the case of wafer A, the preexponential factor  $A$  varies with the bias conditions. The value increases with the field from  $A \sim 1$  for  $V_D = 3$  V up to  $A = 16$  for  $V_D = 5$  V. Using the value of  $A$  for the low bias condition we find  $E_T = 0.39 \pm 0.03$  eV. A possible explanation for variation of the preexponential constant is the presence of an alternative tunneling emission process. The preexponential factor and the activation energy measured in the presence of additional emission mechanisms, such as tunneling, are usually underestimated. The extrapolated value for wafer A therefore should be regarded as a lower bound for the zero-field ionization energy.

The data show that in spite of relatively small apparent activation energies measured in all samples, the correspond-

TABLE I. Parameters of the trapping center.

Sample	$e(0)$ ( $s^{-1}$ )	$\alpha$ ( $V^{-1/2}$ )	$A$ ( $s^{-1} K^{-2}$ )	$E_A$ (eV) <sup>a</sup>	$E_T$ (eV)
A	$0.04 \pm 0.03$	$6.4 \pm 0.4$	1–16	$0.09 \pm 0.02$	$> 0.39 \pm 0.03$
B	$0.02 \pm 0.01$	$5.8 \pm 0.6$	$1.4 \pm 0.5$	$0.065 \pm 0.01$	$0.41 \pm 0.05$
C	$0.003 \pm 0.001$	$6.8 \pm 0.5$	$7 \pm 1$	$0.15 \pm 0.01$	$0.54 \pm 0.05$

<sup>a</sup>Apparent activation energy at  $V_D = 4$  V.



ing trapping center is characterized by the energy level located deep inside the band gap. Variation of the extrapolated values in three wafers is probably due to the presence of alternative emission mechanisms, which affect the value of the preexponential factor  $A$ . Determination of the zero-field ionization energy relies critically on the accuracy of the factor  $A$ . In the case of pronounced variation of the factor  $A$ , the extrapolation to the zero-field ionization energy may result in substantial errors.

### B. Three-dimensional Poole-Frenkel effect

In the consideration of the field-assisted electron emission we used the one-dimensional (1D) PF model. However, the trapping centers are most likely point defects. A three-dimensional (3D) treatment of the Coulomb potential in the uniform field predicts electric field and temperature dependences different from Eq. (4). Following Hartke, the field-assisted emission rate in the spherical case can be expressed,

$$e/e_0 = \left( \frac{kT}{\beta\sqrt{F}} \right)^2 \left\{ 1 + \left[ \left( \frac{\beta\sqrt{F}}{kT} \right) - 1 \right] \exp \left[ \frac{\beta\sqrt{F}}{kT} \right] \right\} + \frac{1}{2}, \quad (5)$$

where  $e_0$  is the emission rate in the absence of the field.<sup>16</sup> The functional dependences of the emission rate on the temperature and the field are more complex as compared to the 1D PF model. We note that for the relatively high fields used in the present experiments ( $10 < \beta\sqrt{F}/kT < 20$ ), this expression can be approximated by a simpler form of the 1D PF effect  $e/e_0 = a \exp[\beta^*\sqrt{F}/kT]$  with a preexponential constant  $a = 0.174$  and a modified constant  $\beta^* = 0.933\beta$ . It allows the use of the classical (1D) PF model, the mathematical form of which is very simple and convenient for the fitting. However, the results of the classical model, namely, the parameters  $A$ ,  $E_T$ , and  $\beta$  require corrections.

The physical meaning of the modified constant  $\beta^*$  can be explained as follows. In the one-dimensional case, the potential lowering in the direction of the field  $\Delta\phi_{PF}$  is well defined, whereas in the spherical case, the barrier lowering depends on the emission direction as  $\Delta\phi_{PF} \cos \theta$ , where  $\theta$  is the angle between the direction of the applied field and the emission direction. Integrated over all angles ( $0 \leq \theta \leq \pi/2$ ), the effective average potential lowering is smaller than  $\Delta\phi_{PF}$ . Therefore, for a given strength of the electric field, the emission enhancement is smaller as compared to the prediction of the 1D PF model. Or, equivalently, the field strength extracted from the emission rate data using the 1D PF model is underestimated by the factor  $\beta/\beta^*$ . The relationship between the applied field and the PF barrier lowering, specifically the coefficient  $\beta$ , must be modified.

The activation energy is deduced from the slope of  $\ln(eT^2)$  plotted as a function of the inverse temperature. Both models practically overlap in the interval of the measured temperatures. Therefore the 1D approximation gives an accurate estimate of the activation energy without any corrections.

The preexponential constant  $a < 1$  implies that for weak fields and high temperatures the disagreement between the 1D and 3D model increases. The classic model predicts a

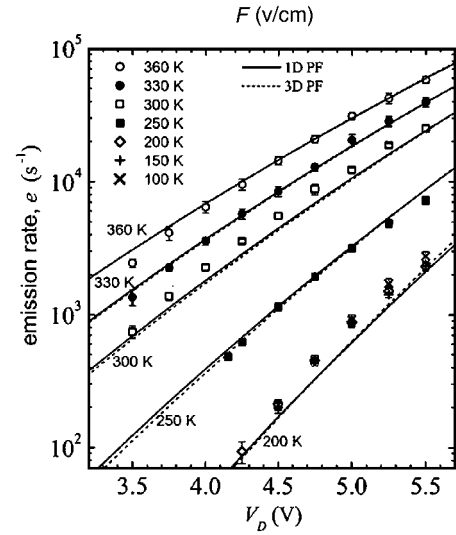


FIG. 6. The emission rate as a function of the gate-drain voltage at different temperatures for sample C. Solid and dashed lines represent the results of the 1D and 3D models.

somewhat lower emission rate as compared to Eq. (5) for  $\beta\sqrt{F}/kT < 5$ . While this regime is not considered in the experiment, extrapolation to  $\beta\sqrt{F}/kT = 0$  using the 1D model results in underestimation of parameter  $A$ . The expression for the emission rate in 1D approximation for the high field regime can be written as

$$e(T, F) = aA^*T^2 \exp \left[ -\frac{E_T - \beta^*\sqrt{F}}{kT} \right]. \quad (6)$$

The experimentally measured emission rate is well described by this equation. However, the preexponential  $aA^*$  constant extracted by fitting the data with Eq. (6) is reduced by the factor of  $a$  as compared to the 3D model.

Finally we compare the experimental results and the results of both models. Figure 6 shows the emission rate as a function of the applied drain voltage for different temperatures. The experimental values are displayed by symbols. The solid lines show the emission rate calculated using 1D PF model [Eq. (6)]. The parameters  $aA^* = 6.9$  and  $E_T = 0.54$ . The PF barrier lowering is expressed in terms of the applied gate-drain potential difference  $\Delta\phi_{PF} = \alpha^*\sqrt{V_D}$ , where  $\alpha^* = \alpha\beta^*/\beta$ . The dashed lines show the results of the three-dimensional PF model with the preexponential factor  $A^* = 54.5$  and the zero-field activation energy  $E_T = 0.54$  eV. The experimental data are well described by both models at temperatures above 250 K. At the lower temperatures, the emission rate stays at a level that is substantially higher than the thermal ionization rate, indicating the importance of direct tunneling.

### C. Trap characteristics

For the deep level trapping centers, the ionization energy (zero field) is mainly determined by the short-range potential.<sup>17,18</sup> Even strong electric field up to  $5 \times 10^6$  V/cm imposes only small perturbation of the trapping potential within the short distance from the center. The electric field, on the other hand, strongly perturbs the long-range potential

as shown in Fig. 1. Therefore, the field enhancement of the thermally activated emission is determined mostly by the long-range potential. The functional form of the electric field dependence observed in the experiment is well explained by the PF effect for the attractive Coulomb potential. Other forms of the long-range potential, for instance, the polarization and the dipole potentials, predict different functional dependences.<sup>19</sup> We can also rule out a  $\delta$ -function potential, since this potential has only a short-range component and the thermal emission is not affected by the electric field. Consequently, the observed PF effect indicates that the trap is an attractive center described by the Coulomb long-range potential.

The form of the long-range potential also determines the probability of electron trapping by the center. The applied electric field therefore can affect the capture cross section. The variation of the cross section in the presence of the field can be attributed to several factors: (i) geometrical shrinkage of the trapping center, (ii) high drift velocity of the conduction electrons, and (iii) high probability of electron tunneling.

Consider a trapping center described by the Coulomb potential. In the uniform electric field, the potential forms a maximum in the direction of the field. The distance between the center of the trap and the maximum decreases as the inverse square root of the applied field. For the field strength of  $10^6$  V/cm, the distance to the maximum is  $\sim 1$  nm. The corresponding equipotential surface forms an ellipsoid elongated in the direction of the field. An electron can be captured only if its trajectory intersects the surface of the ellipsoid, which represents the physical size of the trap. The geometrical cross section of the ellipsoid scales as the inverse of the applied field. In addition, the electron is captured on the trap only if it loses its kinetic energy. The electron therefore has to undergo a scattering event inside the volume of the trap. As the size of the trap decreases, the effective cross section can become significantly smaller than the geometrical size of the trap. The capture cross section can be estimated using the corrected preexponential factor  $A^* = A/a$  (Ref. 9),

$$\sigma = A^* \frac{h^3}{2\sqrt{3}(2\pi)^{3/2} m^* k^2}. \quad (7)$$

For sample C, we find  $\sigma = 0.8 \pm 0.1 \times 10^{-19} \text{ cm}^2$ .

## D. Trap location

Applying the model further, we can estimate the actual field strength in the region of the trapped charge. The ratio  $(\beta^*/\alpha^*)^2$  defines the relationship between the applied potential difference and the field strength. We find that the field enhancement observed experimentally at  $V_D = 5$  V is caused by the field strength of  $3 \pm 1 \times 10^6$  V/cm. There is only one place in the structure, where electric fields of such magnitude exist: directly under the gate terminal. In fact, the field in the barrier under the gate is slightly smaller than the value that follows from the field assisted emission data. We therefore conclude that the active traps are located at the edge of the gate contact at the drain side, where the field is stronger due

to the edge singularity. We also note that the high electric field at the edge results in the highest level of the tunneling current during the filling pulse. Therefore the defect states located in this region are more likely to capture an electron.

## V. SUMMARY

We have described the effect of electric field on the electron emission from the trapping centers in the structure of AlGaIn/GaN HEMTs. We show that dynamics of electrons in and out of the trapping centers is strongly influenced by the electric field in the barrier. The measured characteristics of the emission process unambiguously point to the Poole-Frenkel mechanism. Enhancement of the emission rate in the presence of the field corresponds to the decrease of the apparent activation energy of the trapping center.

From the practical point of view, the understanding of the mechanism of the trapping process allows quantitative characterization of the trapping centers. The PF behavior indicates that the trapping center is described by the long-range attractive Coulomb potential. Consequently, in the presence of the field, the apparent activation energy of the trap decreases and should not be used as a characteristic of the trap. Since the traps are subject to the electric field during the measurements, the zero-field ionization energy can only be extrapolated from the measurements of the apparent activation energy by applying the PF model. We show that the classical (1D) PF model can be used instead of the more complex three-dimensional model in the regime of high electric field. We find that the energy level of the trap is located  $\sim 0.5$  eV below the conduction band minimum, which is substantially deeper compared to the apparent activation energy. Magnitude of the PF effect indicates that the active trapping centers are located in the region of very high electric field exceeding  $10^6$  V/cm. The field of such strength is concentrated at the edge of the gate contact.

<sup>1</sup>J.P. Ibbetson, P.T. Fini, K.D. Ness, S.P. DenBaars, J.S. Speck, and U.K. Mishra, *Appl. Phys. Lett.* **77**, 250 (2000).

<sup>2</sup>B. Jogai, *J. Appl. Phys.* **93**, 1631 (2003).

<sup>3</sup>S.C. Binari, P.B. Klein, and T.E. Kaizer, *Proc. IEEE* **90**, 1048 (2002).

<sup>4</sup>O. Mitrofanov and M. Manfra, *Superlattices Microstruct.* (to be published).

<sup>5</sup>D.V. Lang, *J. Appl. Phys.* **45**, 3023 (1974).

<sup>6</sup>J.G. Simmons, *Phys. Rev.* **155**, 657 (1967).

<sup>7</sup>S. Makram-Ebeid and M. Lannoo, *Phys. Rev. B* **25**, 6406 (1982).

<sup>8</sup>O. Mitrofanov and M. Manfra, *Appl. Phys. Lett.* **84**, 422 (2004).

<sup>9</sup>S.M. Sze, *Physics of Semiconductors* (Wiley, New York, 1981).

<sup>10</sup>N.G. Weimann, M.J. Manfra, and T. Wächtler, *IEEE Electron Device Lett.* **24**, 57 (2003).

<sup>11</sup>M.J. Manfra, N.G. Weimann, O. Mitrofanov, T. Wächtler, and D.M. Tennant, *Phys. Status Solidi A* **200**, 175 (2003).

<sup>12</sup>M.J. Manfra, N.G. Weimann, Y. Baeyens, P. Roux, and D.M. Tennant, *Electron. Lett.* **39**, 694 (2003).

<sup>13</sup>N.G. Weimann, M.J. Manfra, S. Chakraborty, and D.M. Tennant, *IEEE Electron Device Lett.* **23**, 691 (2002).

<sup>14</sup>M.J. Manfra, N.G. Weimann, J.W.P. Hsu, L.N. Pfeiffer, K.W. West, and S.N.G. Chu, *Appl. Phys. Lett.* **81**, 1456 (2002).

<sup>15</sup>O. Mitrofanov, M. Manfra, and N. Weimann, *Appl. Phys. Lett.* **82**, 4361 (2003).

<sup>16</sup>J.L. Hartke, *J. Appl. Phys.* **39**, 4871 (1968).

<sup>17</sup>H.P. Hjalmarson, P. Vogl, D.J. Wolford, and J.D. Dow, *Phys. Rev. Lett.* **44**, 810 (1980).

<sup>18</sup>S.T. Pantelides, *Rev. Mod. Phys.* **50**, 797 (1978).

<sup>19</sup>P.A. Martin, B.G. Streetman, and K. Hess, *J. Appl. Phys.* **52**, 7409 (1981).